Polyhedron 154 (2018) 302–308

Contents lists available at ScienceDirect

Polyhedron

journal homepage: www.elsevier.com/locate/poly

Development of iridium porphyrin arrays by axial coordination through *N*-bidentate ligand: Synthesis and evaluation of the optical, electrochemical and thermal properties

M. Cidália R. Castro [a,*], Arsénio de Sá [a], António M. Fonseca [b], M. Manuela M. Raposo [b], Ana V. Machado [a]

[a] Institute of Polymers and Composites (IPC) and Institute of Nanostructures, Nanomodelling and Nanofabrication (i3N), University of Minho, Campus de Azurém, 4800-058 Guimarães, Portugal
[b] Chemistry Center, University of Minho, Campus de Gualtar, 4710-057 Braga, Portugal

ARTICLE INFO

Article history:
Received 6 June 2018
Accepted 21 July 2018
Available online 31 July 2018

Keywords:
Synthesis
Coordination chemistry
Iridium porphyrin
Axial bipyridine ligand
Optical and redox properties

ABSTRACT

Several organic compounds have been used in optoelectronics devices; porphyrins, due to their interesting optical and electronic properties, have shown an attractive potential to be used on molecular electronics. Among other advantages, porphyrins easily coordinate with several metal ions, which allows the assembly with peripheral or axial ligands introducing new properties to the supramolecular porphyrin. In this work, a new metalloporphyrin system with 5,10,15,20-(tetra-*p*-tolyl)porphyrin (ttp) and iridium(III) where 4,4′-bipyridine (bpy) coordinate in the axial positions was successfully synthetized, through the formation of "shish kebab" structures. This new compound was characterized through ultraviolet–visible, proton nuclear magnetic resonance, Fourier-transform infrared and Raman spectroscopies, thermogravimetry, differential scanning calorimeter and cyclic voltammetry. The introduction of the bpy on the metalloporphyrin moiety exhibited important influence on the optical, thermal and electrochemical properties.

1. Introduction

For several years, porphyrins and metalloporphyrins have attracted high interest from researchers due to their applications in molecular electronics, nonlinear optics, optical data storage, chemical sensors, photovoltaic materials, electrochromic and photocatalytic systems [1–7]. The great interest on porphyrins is related to their properties, in particular their large π-electron conjugation, which allows an effective pathway for electron transport, and small HOMO/LUMO energy gaps, allowing absorption in the visible region that results in exceptional electronic and optical properties [3,8]. Another important characteristic of porphyrins, 18 π-electron aromatic macrocycles, is their ability to accommodate metal ions to form 1:1 metal complexes. The tetradentate anionic porphyrinato system, formed by losing two inner NH protons, is very versatile and can easily coordinate with almost all metal elements of the periodic table. However, the capacity of a porphyrin to coordinate the metal ion is restricted by the space available in the porphyrins' ring core and the ionic radius of the metal ion [9,10]. The porphyrin ring is flexible and is able to assume several conformations. Thus, in the case of 3*d* elements, the ionic radius fits into the porphyrins' ring core forming a planar geometry with the porphyrin, whereas in the case of large ions as some of 4*d* and 5*d* elements, the metal ion is coordinated outside the porphyrin plane forming an octahedral geometry. In both cases the porphyrin sphere is completed with the use of ligands [11–13]. Thus, metalloporphyrins are very useful in the construction of flexible nanometer-sized building blocks for the control of materials properties. Their materials' fundamental properties derived not only from their response to macroscopic effects and interaction with applied electric, magnetic or electromagnetic fields but also from the interaction with other chemical species working as "chemoresponsive" materials [6].

The coordination of metal ions by porphyrins' ring core and axial conjugated ligands is a useful strategy in the construction of multicomponent metalloporphyrin-based molecular complexes, which can be very versatile for the preparation of building block polymers with interesting properties. Metalloporphyrins arrays have, lately, attracted high interest as a new class of porphyrin-based polymers with a wide range of applications, including catalysis, molecular sensors, electronics and new photonics materials, nonlinear optics, electrochromic and transport energy charge, biological and others [6,7,14–16]. Electronic and electrical conductive

* Corresponding author.
E-mail address: cidaliacastro@dep.uminho.pt (M.C.R. Castro).

https://doi.org/10.1016/j.poly.2018.07.035
0277-5387/

properties are the most important characteristics of materials for such applications, thus they should be taken into account when develop novel metalloporphyrins systems. "Shish kebab" structures have been investigated since the late 1970s and are related to coordination polymers based on metalloporphyrins linked through axial coordination of π-electron-containing bridging ligands [17–19]. The conductivity of these multicomponent systems depends on large-scale on the interaction between the metal's d_π orbitals and π^* level of the axial ligand and the presence of electron donor/acceptor pairs. It is known that the large π system of metalloporphyrin origins a HOMO and LUMO gap generally around 2 eV, however, metalloporphyrins self-assemble systems are able to narrow this energy gap, leading to improved conductivity properties [6,19,20]. Furthermore, the self-assembly of metalloporphyrins depends on the degree of the delocalization between the metal ion and the porphyrin and consequently the relative orbital energies are affected by the coordination with a specific ligand. Iridium complexes have attracted more attention than other common metals and *d*-block metals due to their larger spin–orbit constant, heavier atomic mass and their emission energies that can be easily adjusted across the visible spectrum [21]. Iridium porphyrins in particular, has been the target of great notoriety on the part of researchers due to their interesting properties in a wide range of applications, including catalysis, sensors and switching layers in electronic devices [21–23].

Recently, we published two new iridium-porphyrin complexes where the metal center was stabilized with Cl and CO ligands [24,25]. Therefore, and based on these results, this work investigates the preparation of a "shish kebab" structures of a metalloporphyrin system. 5,10,15,20-(Tetra-*p*-tolyl)porphyrin (ttp) was used to coordinate iridium(III) and 4,4-bipydirine (bpy) in order to promote the formation of the "shish kebab" structure. To the best of our knowledge, this is the first report of a stable iridium porphyrin with such a long conjugated bidentate spacer. The ratio between the metalloporphyrin and the bipyridine was fixed in 1:8 [Ir(ttp):(byp)], in which the chloride anion from the start material balances the complex charge. The metalloporphyrin arrays were characterized by ultraviolet–visible (UV–Vis), proton nuclear magnetic resonance (^{1}H NMR), Fourier-transform infrared (FTIR) and Raman spectroscopies, thermogravimetry (TGA), differential scanning calorimeter (DSC) and cyclic voltammetry (CV).

2. Experimental

2.1. Materials and reagents

The 5,10,15,20-(tetra-*p*-tolyl)porphyrin (ttp) (98%) was purchase from Porphychem. Chloro(1,5-cyclooctadiene)iridium(I) dimer {[Ir(COD)Cl]$_2$, 97%} and tetrabutylammonium tetrafluoroborate (99%) [NBu_4][BF_4] were acquired from Sigma-Aldrich. 4,4′-bipyridine (98%) was obtained from Alfa Aesar. The solvents used, xylene (99.9%), toluene (99.99%), dichloromethane (99.99%) (DCM), *N*,*N*-dimethylformamide (99.99%) (DMF) and *n*-hexane (98.08%), were bought from Fisher Chemical and used without further purification. Thin layer chromatography was performed in pre-coated silica gel 60 F-254 plates obtained from Merck and column chromatography was accomplished in silica gel 60 M (0.040–0.060 mm) from Acros Organics.

2.2. Measurements and instrumentation

All the compounds were characterized by ^{1}H NMR spectroscopy using a Bruker Avance III, 400 MHz, and deutered chloroform ($CDCl_3$) as solvent. The spectra were internally referenced to the residual proton tetramethylsilane (TMS, δ = 0.00 ppm) and the chemical shifts (δ) are reported as part per million (ppm).

Absorption spectra were measured using a Shimadzu UV-2401PC UV–Vis spectrophotometer in dichloromethane (DCM) in a range between 250 and 700 nm.

Mass spectrometry (MALDI-TOF) was performed using an Autoflex III smartbeam MALDI-TOF mass spectrometer Bruker Daltonik, operating in reflector positive ion mode. Ions were formed upon irradiation by a smart beam nitrogen laser (337 nm) using an accelerating potential of 20 kV and a frequency of 200 Hz. Averaging 1500 laser shots collected across the whole sample spot surface by rastering in the range *m*/*z* 700–4000 produced each mass spectrum. All spectra were acquired and treated using the FlexControl 3.0 and FlexAnalysis 3.0 softwares (Bruker Daltonik, Bremen, Germany), respectively.

Transmission Infrared spectroscopy (FTIR) was made on a 4100-Jasco in the range between 4000 and 400 cm^{-1} using 32 scans. Samples were analysed by deposition of a liquid film (DCM) on a NaCl cell and after solvent evaporation. Raman spectroscopy was carried out on a LabRAM HR Evolution Raman spectrometer (Horiba Scientific, France) coupled with a Horiba Scientific's Labspec 6 spectroscopy set which provides not only a complete instrument control but also data processing. The Raman spectra were acquired with a 532 nm laser excitation wavelength (0.1% laser intensity), with an acquisition time and accumulation of 30 s in a range between 500 and 1800 cm^{-1}.

Thermal studies were carried out using thermogravimetric analysis performed in a TGA Q500 (TA Instruments) and differential scanning calorimetry analysis performed in a Perkin Elmer DSC 7 under N_2 atmosphere at a heating rate of 10 °C/min on a temperature range of 40–700 °C and 40–500 °C, respectively.

Cyclic voltammetry (CV) was accomplished with a three-electrode arrangement, whereby the potential relative to a silver-wire reference electrode is scanned at a vitreous carbon disc-working electrode (areas = 0.049 cm^2), while the resulting current flow through a platinum-wire auxiliary electrode is monitored in a quiescent solution. This study was performed at room temperature in *N*,*N*-dimethylformamide (DMF) solutions of the target compound ([C] = 0.001 M) with 0.1 M of tetrabutylammonium tetrafluoroborate [NBu_4][BF_4] as supporting electrolyte. All the solutions were studied at different scan rates (20, 50, 100 and 200 mV s^{-1}) in the absence of oxygen and all the relevant data is presented with respect to ferrocenium/ferrocene (fc^+/fc) as an internal reference (E_{Fe} = 0 mV) for ease comparison.

2.3. Synthesis of chloro(5,10,15,20-tetratolylporphyrinato)carbonyliridium(III) [Ir(ttp)Cl(CO)] **1**

This compound was synthesized according to the method reported in literature [24,26–28]. [Ir(COD)Cl]$_2$ (0.39 mmol) was added to a H_2ttp (0.26 mmol) solution in xylene (100 mL), and the mixture was refluxed for 4 days. The solvent was removed by evaporation under vacuum. The reaction crude was purified by silica gel column chromatography using a mixture of n-hexane and dichloromethane of increasing polarity as eluent. The pure product was obtained by recrystallization from dichloromethane/hexane as a purple solid in 67% yield.

^{1}H NMR ($CDCl_3$) δ ppm = 2.74 (s, 12H, 4×C*H*$_3$), 7.59 (dd, 8H, *J* = 8.4 and *J* = 0.4 Hz, H_2 and H_6), 8.15 (dd, 8H, *J* = 8.4 and *J* = 1.6 Hz, H_3 and H_5), 8.97 (s, 8H, β-py) ppm. UV–Vis (CH_2Cl_2): $\lambda_{máx}$ = 421 [7.29×10^7 (log ε 7.86)], 497 [5.50×10^6 (log ε 6.74)], 533 [3.98×10^7 (log ε 7.60)], 567 [1.04×10^7 (log ε 7.02)] nm. MS (MALDI-TOF): *m*/*z* 925.23 calculated for $C_{49}H_{36}ClIrN_4O$; found *m*/*z* 859.32 [$C_{48}H_{36}IrN_4$]; *m*/*z* 887.26 [$C_{49}H_{36}IrN_4O$].

2.4. Synthesis of (5,10,15,20-tetratolylporphyrinato) (bipyridine)$_2$iridium(III) [Ir(ttp)(bipyridine)$_2$] **2**

The [Ir(ttp)(bipyridine)$_2$] arrays were synthesized through the addition of excess 4,4′-bipyridine (0.43 mmol) to a solution of [Ir(ttp)Cl(CO)] **1** (0.054 mmol) in toluene (15 mL). The reaction mixture was refluxed for 4 days with stirring. After this time and after cool till room temperature the crude was dried under vacuum and purified by silica gel column chromatography using a mixture of *n*-hexane and dichloromethane of increasing polarity as eluent. The pure product was obtained by recrystallization from dichloromethane/*n*-hexane as dark red solid in 36% yield.

^{1}H NMR ($CDCl_3$) δ ppm = 2.64 (s, 4H, bpy) 2.70 (s, 12H, 4×CH_3), 5.69 (d, 4H, *J* = 6.8 Hz, bpy), 6.89 (d, 4H, *J* = 3.6 Hz, bpy), 7.58 (d, 8H, *J* = 7.8 Hz, H_2 and H_6), 8.02 (d, 8H, *J* = 7.8 Hz, H_3 and H_5), 8.27 (s, 4H, bpy), 8.93 (s, 8H, β-py) ppm. UV–Vis (CH_2Cl_2): $\lambda_{máx}$ = 412 [1.06 × 10^6 (log ε 5.03)], 524 [1.00 × 10^4 (log ε 4.00)] nm. FTIR ν cm^{-1} = 3023, 2920, 1644, 1593, 1488, 1408, 1355, 1312, 1076, 1016, 800, 715, 630 cm^{-1}. Raman cm^{-1} = 416, 712, 809, 838, 1023, 1085, 1239, 1336, 1371, 1493, 1526, 1552, 1580 cm^{-1}. MS (MALDI-TOF): *m*/*z* 1173.39 calculated for $C_{68}H_{52}IrN_8$; found *m*/*z* 1173.36 [$C_{68}H_{52}IrN_8$]; *m*/*z* 861.23 [$C_{48}H_{36}IrN_4$].

3. Results and discussion

An initial study was performed to evaluate the optimal ratio between metalloporphyrin [Ir(ttp)Cl(CO)] **1** and 4,4′-bipyridine (bpy) in order to synthesize (5,10,15,20-(tetratolylporphyrinato) (bipyridine)$_2$iridium(III) [Ir(ttp)(bipyridine)$_2$] **2** (Scheme 1). It was noticed that a ratio higher than 1:5 [Ir(ttp):bpy] favors the formation of [Ir(ttp)(bipyridine)$_2$] **2**. Based on our results and taking into account the literature data [29], the ratio for these reaction was set 1:8 [Ir(ttp):bpy].

3.1. UV–Visible spectroscopy

Fig. 1 shows the UV–Vis spectra of [Ir(ttp)Cl(CO)] **1**, [Ir(ttp) (bipyridine)$_2$] **2** and bipyridine in dichloromethane at room temperature. The spectra have an extensive measurement range to allow the identification of the absorption bands related to the non-coordinated bipyridine (around 238 nm) and coordinated (around 260 nm). The absorption bands between 200 and 300 nm, observed on complex **1** and cover-up by complex **2**, may be related to charge-transfer processes between the porphyrin and the metal ion. These charge-transfer processes are detected

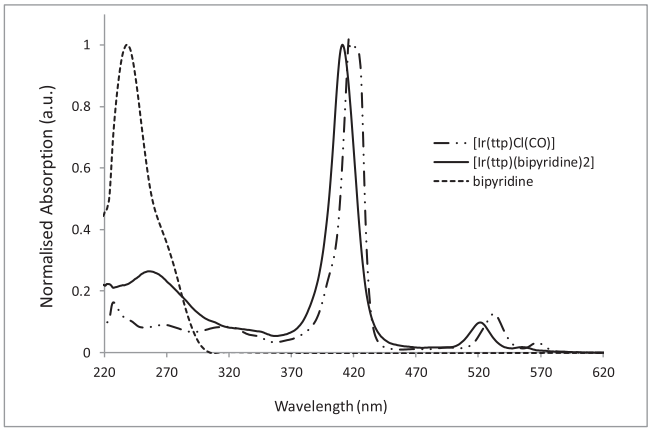

Fig. 1. Normalized UV–Vis spectral of [Ir(ttp)Cl(CO)] **1** and [Ir(ttp)(bipyridine)$_2$] **2** in dichloromethane at room temperature.

particularly with transition metals with open *d*-shells [30,31]. According to the UV–Vis spectra (Fig. 1), the axial coordination by bpy increases these types of processes, which is consistent with the required properties for the development of optoelectronic materials. During the reaction of the free porphyrin with the metal it was noticed a bathochromic shift and a decrease in the number of Q bands, related to the change of a rectangular symmetry in the free porphyrin to a nonplanar deformation in the metal complex. However, the compound **2**′s spectrum (Fig. 1) reveals a hypsochromic shift of the Soret and Q band relative to compound **1**. When the ligands coordinating the iridium are replaced by bipyridine, a blue shift of the Soret and Q bands was detected, which can result from the recovery of the planar geometry and the symmetry of the new metal complex [32].

3.2. Proton NMR spectroscopy

^{1}H NMR experiments were carried out to characterize the structure of the metal complex and to better understand the influence of the new axial ligand in the metalloporphyrin system. Iridium (III) complexes are diamagnetic, with low-spin, and generally have an octahedral geometry.

NMR spectra demonstrate that the resonances concerning the porphyrin core of the [Ir(ttp)bipyridine$_2$] **2** are upfield, compared to **1** (Table 1). This means that the exchange of the CO and Cl ligands by bipyridine moiety results in a greater protection of the

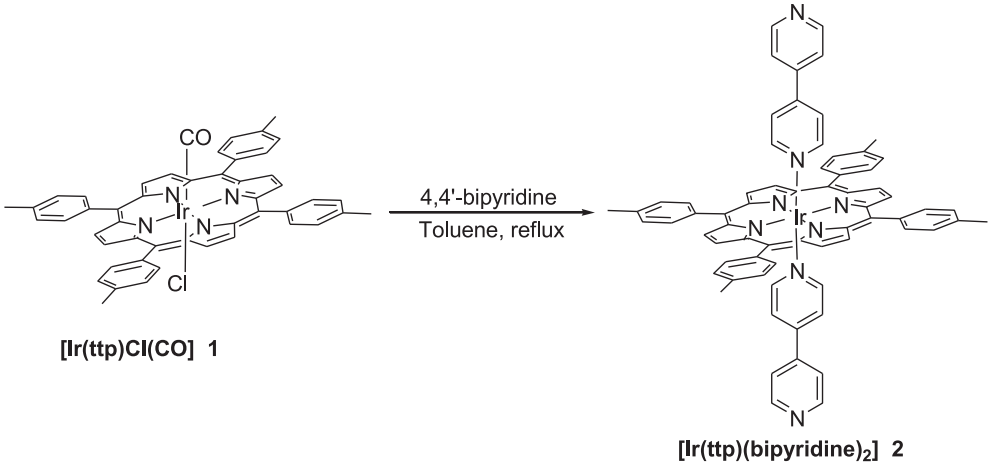

Scheme 1. Synthesis of [Ir(ttp)(bipyridine)$_2$] **2** based on a ligand exchange reaction with 4,4′-bipyridine.

Table 1
Selected ^{1}H NMR spectra chemical shifts (ppm) for the metal complexes **1** and **2**.

Compound	CH_3(tolyl)	$H_{\beta\text{-pyrrol}}$	$H_{o\text{-tolyl}}$	$H_{m\text{-tolyl}}$
1	2.74	8.97	7.59	8.15
2	2.69	8.93	7.58	8.02

tolyl protons and the β-pyrrolic protons. The twelve equivalent protons of the methyl group present on tolyl resonate as a singlet at 2.74 ppm for compound **1** and at 2.69 ppm for compound **2**. The protons in tolyl groups' resonances appear, for compound **1**, as two double doublets at 7.59 and 8.15 ppm, whereas for compound **2** appear as doublets at 7.58 and 8.02 ppm. The eight equivalent β-pyrrolic protons appear as a singlet and exhibit downfield chemical shifts, being clearly visible at 8.97 ppm for compound **1** and at 8.93 ppm for compound **2**. The non-coordinate 4,4′-bipyridine exhibits two doublets resonances at 8.75 and 7.53 ppm, where each doublet is related to 4 equiv. protons. When coordinating, the metal ion resonances appear at higher magnetic fields and as four different signals at 2.64, 5.70, 6.89 and 8.27 ppm. The integration of each of these signals is related to 4 equiv. protons, indicating the presence of two bipyridine molecules coordinating the metal ion. This means that the reaction between [Ir(ttp)Cl(CO)] and bipyridine results in formation of the metalloporphyrin where two bipyridine molecules are coordinated to the iridium(III) ion in the axial position.

3.3. Mass spectrometry data (MALDI-TOF MS)

MS spectra of MALDI-TOF experiments for compounds **1** and **2** are shown in Fig. 2 and some principal peaks were characterized: the molecular ion of the moiety $[Ir(ttp)(bipyridine)_2]^+$ appears at 1173.3 and the molecular ion for moiety $[Ir(ttp)]^+$ appears at 861.2. Additionally, it is possible to identify $[Ir(ttp) + Cl]^+$ and $[Ir(ttp) + CO]^+$ species at m/z 896.2 and 887.2, respectively. The high correlation amongst the calculated and measured m/z values of each fragments peaks allows to confirm the axial coordination of two bipyridine molecules to the iridium metal center on the porphyrin cavity. These results are in agreement with the structure identified by ^{1}H NMR, where the upfield shifting proton resonances of ligand may be due to the shielding effect caused by the porphyrin ring current and indicate of metalloporphyrin self-assembly [16,22,33].

3.4. Infrared spectroscopy

The IR spectra for [Ir(ttp)Cl(CO)] **1**, $[Ir(ttp)(bipyridine)_2]$ **2** and bipyridine are presented in Fig. 3 and corroborate the presence of bipyridine in the coordination shell of iridium(III).

The success of this reaction was evidenced essentially by the wavenumber corresponding to the stretching of the C–N and C–C bonds, of the bipyridine moiety, around 1593, 1470 and 1407 cm^{-1}, and the absence of the band of CO at 2045 cm^{-1} [16,29]. The axial coordination of aza conjugated ligands, as bipyridine, has influence on the complexes vibrational waves, where the C═C stretch either on phenyl and porphyrin, the C–H bend in the phenyl and the C–N stretch in porphyrin are shifted to lower or higher energies [16,34]. The absence of a vibrational band at around 3300 cm^{-1}, typical of N–H vibrations, indicates that no demetallation occurred, which prove the stability of the metal complex.

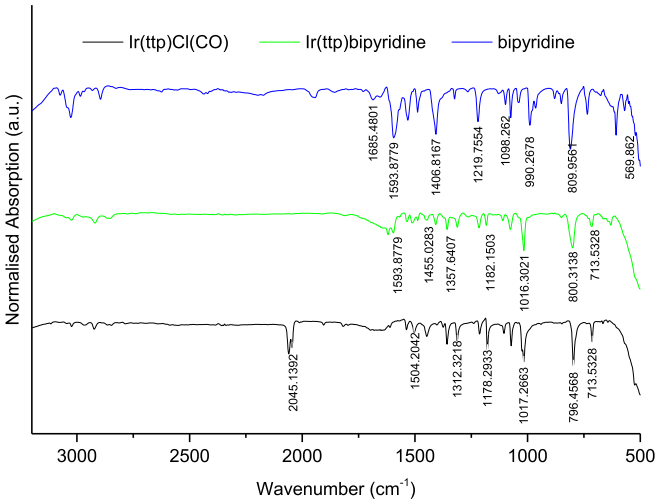

Fig. 3. FTIR spectra of [Ir(ttp)Cl(CO)] **1**, $[Ir(ttp)(bipyridine)_2]$ **2** and bipyridine.

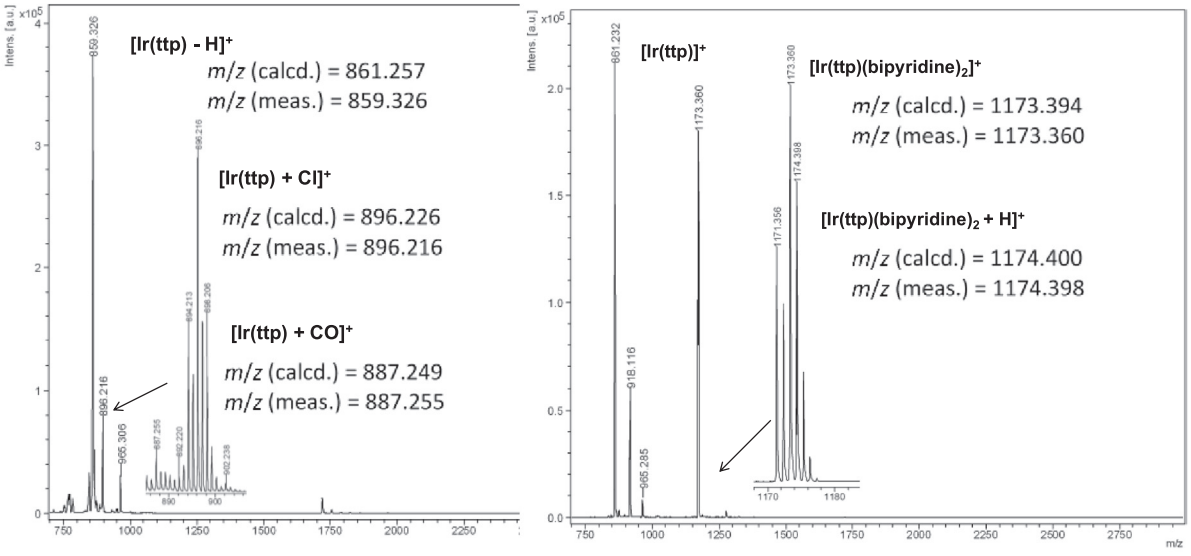

Fig. 2. Positive MALDI-TOF mass spectra for [Ir(ttp)Cl(CO)] **1** (left) and $[Ir(ttp)(bipyridine)_2]$ (right) **2**.

3.5. Raman spectroscopy

Raman spectroscopy was performed to complement the FTIR analysis (Fig. 4). The spectra exhibit a band at 419 cm^{-1}, which is related to the iridium(III) coordinated in the porphyrin's core. Comparing each spectrum, it was noticed a slight deviation of the peaks between 1000 and 1300 cm^{-1} either to higher or lower wavelength on [Ir(ttp)(bipyridine$_2$)] **2** spectrum. This corresponds to the different molecular vibrations of the porphyrin nucleus of compound **2**, which can be associated to the change of the ligands that affect bonds strength and symmetry, as it was observed in the UV–Vis studies. The bands between 1400 and 1600 cm^{-1} are frequently attributed to the stretching frequencies of C_β–$C_{\beta'}$ bonds on the pyrrole ring and the bonds between the C_α and the quaternary carbon next to the pyrrole ring (C_{meso}). The region between 1200 and 1370 cm^{-1} is usually attributed to the stretching waves of the bonds between C_α–C_β and C_α–N. The band around 1550 cm^{-1} is imputed to β-pyrrolic carbon stretching frequencies. These results are in agreement with those reported in the literature for similar porphyrins [24,35].

3.6. Thermal characterization

[Ir(ttp)Cl(CO)] **1** (Fig. 5a) presents two onset degradation temperatures, one around 386 °C, with a weight loss up to 9%, and the other around 551 °C, with a weight loss up to 4% (Fig. 5a). While the first degradation step is related to the loss of the tolyl groups, the second is related to the degradation of the porphyrin skeleton [24]. [Ir(ttp)(bipyridine$_2$)] **2** has lower thermal stability than **1** (Fig. 5a), which may be induced by the presence of bipyridine. The thermogram starts with a slight weight loss (2%) around 55 °C up to 160 °C, possibly related to the loss of the crystallization water followed and solvents residues, and three degradation steps. The first at 240 °C, with a weight loss up to 14% seems to be related to the degradation of bipyridine. The second at 341 °C, with a mass loss up to 6%, is related to the degradation of the tolyl groups. At 400 °C (7% weight loss) occurs a third step due to the porphyrin degradation. It is important to notice that in the temperature range used, the complex **1** and **2** do not undergo complete degradation, only 12% and 34% weight loss, respectively. The residual weight, 88% for compound **1** and 66% for compound **2** was found at 700 °C. The DSC thermogram of compound **2** indicates the corresponding four decomposition temperatures at 78 °C, 267 °C, 362 °C and 422 °C (Fig. 5b). The endothermic peaks are due to the cleavage and decomposition of the coordinated bipyridine to the metal, cleavage of the metal from the porphyrin, the cleavage and decomposition of the tolyl group and finally the decomposition of porphyrin core [36–38].

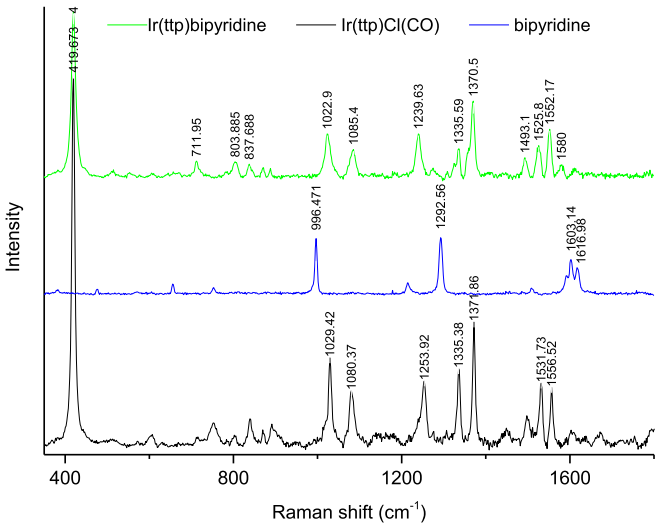

Fig. 4. Raman spectra of [Ir(ttp)Cl(CO)] **1**, [Ir(ttp)(bipyridine$_2$)] **2** and bipyridine.

3.7. Cyclic voltammetry

The electrochemical behaviour of complex [Ir(ttp)Cl(CO)] **1** and [Ir(ttp)(bipyridine$_2$)] **2** was studied trough cyclic voltammetry using tetrabutylammonium tetrafluoroborate [NBu_4][BF_4] as supporting electrolyte in DMF under argon atmosphere. All the known metalloporphyrins are electroactive; thus, cyclic voltammetry is a widely used technique to determine the gap between energy levels for these compounds and to study how the position of the HOMO and LUMO molecular orbitals affects their performance. It is well known that the redox potential of metalloporphyrins is influenced by the nature of the macrocycle and metal ion, complex's geometry, and axial ligands [39].

The redox processes observed in the ttp porphyrin is related to the reduction of the tetraphenylporphyrins macrocycle. The porphyrin can be reversible oxidized in one electron-transfer steps to yield the formation of porphyrin π cation radicals and dications or can be reduced in one electron-transfer steps to produce porphyrin π anionic radicals and dianions [39–42]. The incorporation of a central metal, for instance iridium, causes undoubtedly important changes on the cyclic voltammograms. These differences are essentially due to the strong interactions between the *d* electrons of metal ion and electrons of nitrogen atoms on the porphyrin

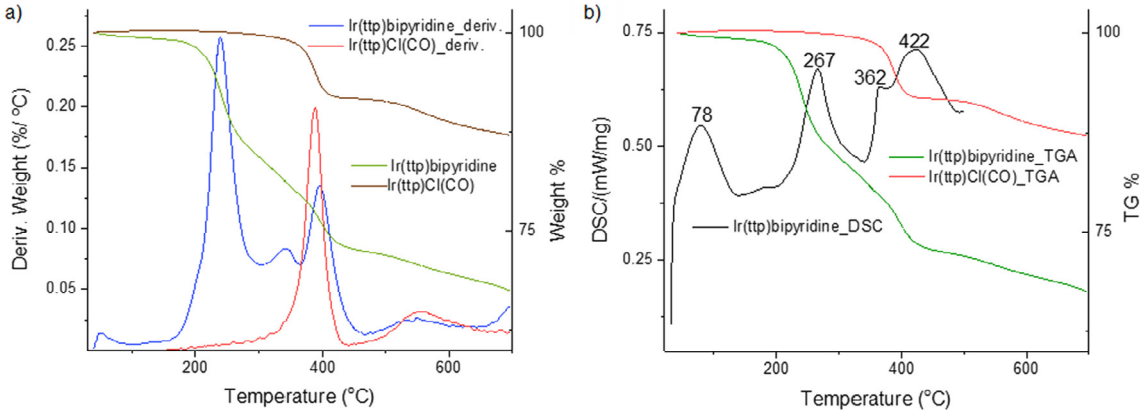

Fig. 5. TGA and DSC curves for compounds [Ir(ttp)Cl(CO)] **1** and [Ir(ttp)(bipyridine$_2$)] **2**.

Table 2
Electrochemical data for ttp, [Ir(ttp)Cl(CO)] **1**, [Ir(ttp)(bipyridine)$_2$] **2** and bipyridine.

Compound	Reduction[a]				Oxidation[a]		$-E_{HOMO}$[b] (eV)	$-E_{LUMO}$[c] (eV)	Band Gap[c] (eV)
	$-^1E_{pc}$ (V)	$-^2E_{pc}$ (V)	$-^3E_{pc}$ (V)	$-^4E_{pc}$ (V)	$^1E_{pa}$ (V)	$^2E_{pa}$ (V)			
ttp	1.60	2.20	2.49	–	0.58	0.81	4.97	2.79	2.18
1	1.61	2.12	2.56	–	0.78	–	4.92	2.78	2.14
2	1.60	2.07	2.23	2.71	0.49	0.83	4.88	2.79	2.09
Bipyridine	2.41	2.82	–	–	0.57	–	–	–	–

[a] Measurements made in dry DMF containing 1.0 mM in each compounds and 0.1 M [NBu_4][BF_4] as base electrolyte at a carbon working electrode with a scan rate of 0.1 V s^{-1}. All *E* values are quoted in volts vs the ferrocenium/ferrocene-couple. E_{pc} and E_{pa} correspond to the cathodic and anodic peak potentials, respectively.
[b] $E_{HOMO} = -(4.39 + E_{ox})$ (eV) and $E_{LUMO} = -(E_{red} + 4.39)$ (eV) [45].
[c] Difference between the onset potentials of the oxidation and reduction peaks.

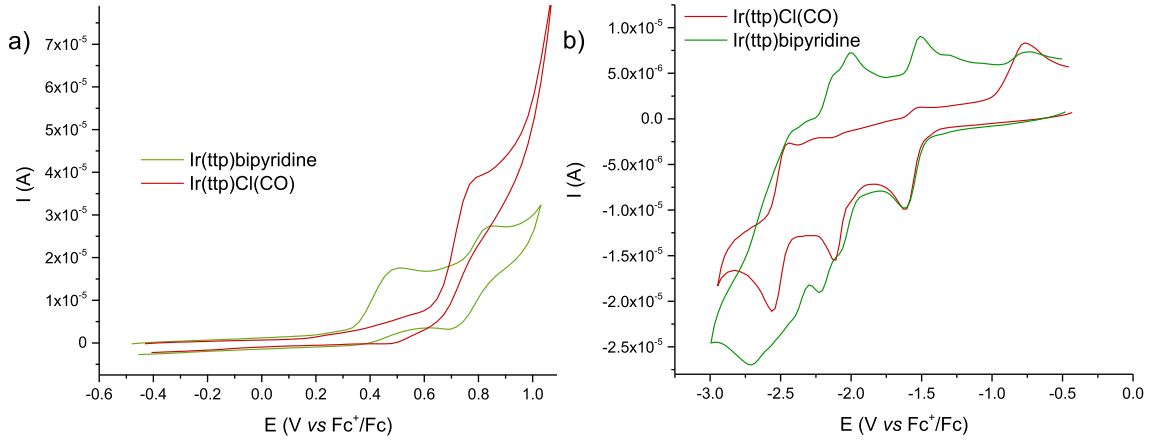

Fig. 6. [Ir(ttp)Cl(CO)] **1** and [Ir(ttp)(bipyridine)$_2$] **2** cyclic voltammograms (a) positive scan of potential and (b) negative scan of potential, performed in DMF using ferrocenium/ferrocene as internal reference and at a scan rate of 100 mV/s.

macrocycle, and also due to the character of the axial ligands [40,43].

Specifically, in this case, the presence of iridium(III) coordinated by Cl and CO in the axial positions results in considerable changes on the porphyrin macrocycle. Electrochemical data of the ttp porphyrin are present in Table 2. The redox process of ttp is in agreement with the electrochemical results of similar compounds, i.e., the redox process *via* two electrons at the conjugated macrocycle gives π-cation radicals/dications and π-anions radicals/dianions [39,44]. Two redox process at 0.58 and 0.81 V (*vs.* fc$^+$/fc) corresponding to the oxidation of porphyrin ring by formation of cation radical. On the ttp reduction it is detected two reversible reduction processes at −1.60 and −2.20 V (*vs.* fc$^+$/fc). The metalation of the free ttp leads to significant shifts of the characteristic reduction and oxidation potentials values, being observed either on [Ir(ttp)Cl(CO)] **1** or [Ir(ttp)(bipirydine)$_2$] **2** voltammograms, Table 2, Figs. 6 and 7. This shift is possibly due to the global contribution of both metal and axial ligands. The electrochemical study of [Ir(ttp)Cl(CO)] **1** (Fig. 6), presents an oxidation process at 0.78 V (*vs.* fc$^+$/fc) and three reduction processes, one partially reversible at −1.61 V (*vs.* fc$^+$/fc), another irreversible process at −2.12 V (*vs.* fc$^+$/fc) and one reversible process at −2.56 V (*vs.* fc$^+$/fc). Usually, in the

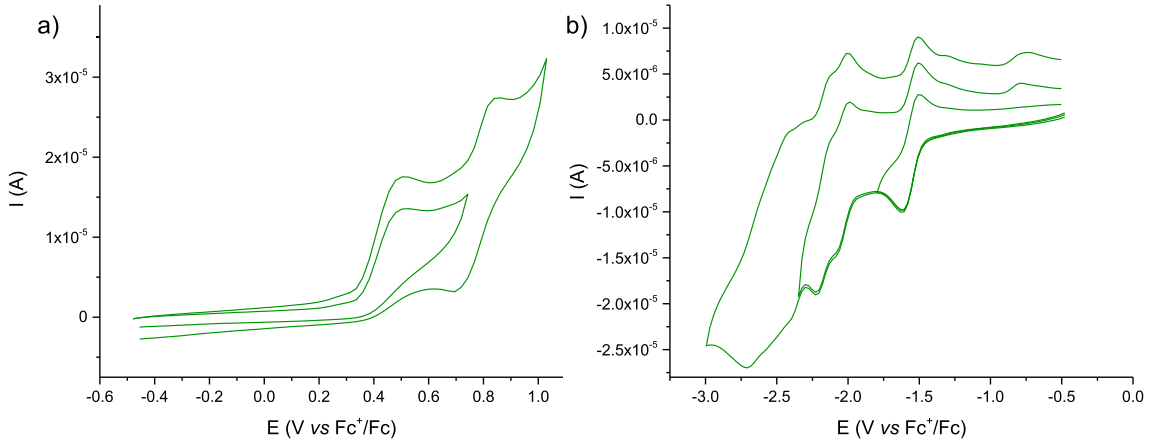

Fig. 7. [Ir(ttp)(bipyridine)$_2$] **2** cyclic voltammograms (a) positive scan of potential and (b) negative scan of potential, performed in DMF using ferrocenium/ferrocene as internal reference and at a scan rate of 100 mV/s.

electrochemical studies of metalloporphyrins are observed two redox processes corresponding to the metal-centered and ring-centered processes. However, for metalloporphyrins such as [Ir(porphyrin)Cl(CO)] only the ring-centered process is observed [43].

The coordination of the *N*-donor ligands, as bipyridine, has a major effect on the redox potentials. Comparing to Cl and CO ligands, systems bearing electron rich heterocycles are easier to oxidize due to the stronger electron-donating ability of the system, resulting in a higher HOMO energy level [39,43]. [Ir(ttp)(bipyridine)$_2$] **2** oxidation (Figs. 6a and 7a) exhibits one irreversible redox process at 0.49 V (*vs.* fc$^+$/fc) which corresponds to the bipyridine oxidation and one reversible redox process at 0.83 V (*vs.* fc$^+$/fc) associated to the porphyrin oxidation, resulting from the relocated π and π^* levels of the highly conjugated metalloporphyrin. On the negative potential scan (Figs. 6b and 7b), it is possible to observe four reduction processes at −1.61, −2.07, −2.23 and −2.71 V (*vs.* fc$^+$/fc) with anodic counterpart. The shift observed on potentials redox data for compound [Ir(ttp)(bipyridine)$_2$] **2** are due to the coordination of the bipyridine.

The band gaps were calculated from the potentials of the anodic and cathodic processes (Table 2). The results are in agreement with those of similar tetraphenylporphyrins (HOMO–LUMO gap energy = 2.25 ± 0.15 eV) [43].

Lower band gap values are indicative of greater π-delocalization, which means that, as expected, the coordination of bipyridine to the macrocycle (complex **2**, with a band gap of 2.09 eV) results in higher conjugation than CO and Cl (complex **1**, with a band gap of 2.14 eV). Moreover, the coordination of bipyridine ligands affects complex's geometry, as already shown on the UV–Vis studies, reducing the distortion, which also decreases the band gap.

4. Conclusions

The synthesis of porphyrin-based iridium(III) complexes, by replacement of CO and Cl by conjugated bipyridine on the precursor metalloporphyrin **1**, was successfully achieved using an experimental procedure at high boiling temperatures. The synthetized [Ir(ttp)(bipyridine)$_2$] **2** was characterized through several techniques, including UV–Vis, ^{1}H NMR, FTIR, Raman, MALDI-TOF, TGA, DSC and cyclic voltammetry. The results showed that these complexes are highly conjugated and diamagnetic, present a six-coordinated Ir(III), probably with an octahedral geometry, where the *N*-donor atoms of bipyridine species occupy the axial positions. The UV–Vis study of complex **2** showed blue shifted Soret and Q bands, which can be attributed to the recovery planarity of the metalloporphyrin macrocycle. Although, TGA studies shows that [Ir(ttp)(bipyridine)$_2$] **2** has a lower thermal stability than complex **1**, and cyclic voltammetry reveals a lower HOMO–LUMO gap energy (band gap) for complex **2**, which represents higher efficiency in the transport of electrons and energy. Therefore, the developed porphyrin-based iridium(III) complexes, demonstrated to have great potential for optoelectronic applications.

Acknowledgements

The authors acknowledge the Portuguese Foundation of Science and Technology (TSSiPRO – TECHNOLOGIES FOR SUSTAINABLE AND SMART INNOVATIVE PRODUCTS – NORTE-01-0145-FEDER-000015) and UID/CTM/50025/2013 for the financial support.

References

[1] L.-L. Li, E.W.-G. Diau, Chem. Soc. Rev. 42 (2013) 291–304.
[2] T. Higashino, H. Imahori, Dalton Trans. 44 (2015) 448–463.
[3] M. Jurow, A.E. Schuckman, J.D. Batteas, C.M. Drain, Coord. Chem. Rev. 254 (2010) 2297–2310.
[4] M. Calvete, G.Y. Yang, M. Hanack, Synth. Met. 141 (2004) 231–243.
[5] Y. Chen, A. Li, Z.-H. Huang, L.-N. Wang, F. Kang, Nanomaterials 6 (2016) 51.
[6] K.S. Suslick, N.A. Rakow, M.E. Kosal, J.-H. Chou, J. Porphyrins Phthalocyanines 04 (2000) 407–413.
[7] J.-H. Chou, M.E. Kosal, H.S. Nalwa, N.A. Rakow, K.S. Suslick, in: Urbana, Vol. 51, scs.illinois.edu, 2000, p. 61801.
[8] S. Fujii, S. Marqués-González, J.-Y. Shin, H. Shinokubo, T. Masuda, T. Nishino, N. P. Arasu, H. Vázquez, M. Kiguchi, Nat. Commun. 8 (2017) 15984.
[9] K.M. Kadish, K.M. Smith, R. Guilard, The Porphyrin Handbook: Inorganic, Organometallic and Coordination Chemistry, Vol. 3, Elsevier, 2000.
[10] I. Bouamaied, T. Coskun, E. Stulz, in: Non-Covalent Multi-Porphyrin Assemblies, Springer Berlin Heidelberg, Berlin, Heidelberg, 2006, pp. 1–47.
[11] T.P. Wijesekera, D. Dolphin, in: Metalloporphyrins in Catalytic Oxidations, 1994, pp. 193–239.
[12] J.M. Gottfried, Surf. Sci. Rep. 70 (2015) 259–379.
[13] Z. Valicsek, O. Horváth, Microchem. J. 107 (2013) 47–62.
[14] I. Beletskaya, V.S. Tyurin, A.Y. Tsivadze, R. Guilard, C. Stern, Chem. Rev. 109 (2009) 1659–1713.
[15] L.P. Cook, G. Brewer, W. Wong-Ng, Crystals 7 (2017) 223.
[16] S. Nasri, I. Zahou, I. Turowska-Tyrk, T. Roisnel, F. Loiseau, E. Saint-Amant, H. Nasri, Eur. J. Inorg. Chem. 2016 (2016) 5004–5019.
[17] A. Winter, U.S. Schubert, Chem. Soc. Rev. 45 (2016) 5311–5357.
[18] S.A. Ikbal, S. Brahma, S.P. Rath, Inorg. Chem. 51 (2012) 9666–9676.
[19] J.P. Collman, J.T. McDevitt, K. Kim, J.M. Garner, M.B. Zisk, C.R. Leidner, G.T. Yee, J.W. Prodolliet, W.A. Little, in: V.Z. Kresin, W.A. Little (Eds.), Organic Superconductivity, Springer, Boston, MA, US, 1990, pp. 359–366.
[20] Z.L. Dunn, M.A. Hammer, B.J. Topham, T.M. Perrine, J. Phys. Chem. C 121 (2017) 12018–12024.
[21] A.F. Henwood, E. Zysman-Colman, in: E. Zysman-Colman (Ed.), Iridium(III) in Optoelectronic and Photonics Applications, 2017, pp. 275–357.
[22] W. Sinha, L. Ravotto, P. Ceroni, S. Kar, Dalton Trans. 44 (2015) 17767–17773.
[23] T.O. Dairo, L.K. Woo, Organometallics 36 (2017) 927–934.
[24] A. Delgado-Lima, J.P. Borges, I.M. Ferreira, A.V. Machado, Mat. Today Commun. 11 (2017) 26–37.
[25] A. Delgado-Lima, A.M. Fonseca, A.V. Machado, Mat. Lett. 200 (2017) 6–9.
[26] S.K. Yeung, K.S. Chan, Organometallics 24 (2005) 6426–6430.
[27] T.D. Lash, K. Pokharel, M. Zeller, G.M. Ferrence, Chem. Commun. 48 (2012) 11793–11795.
[28] H. Ogoshi, J.-I. Setsune, Z.-I. Yoshida, J. Organomet. Chem. 159 (1978) 317–328.
[29] A. Mansour, Y. Belghith, M.S. Belkhiria, A. Bujacz, V. Guérineau, H. Nasri, J. Porphyrins Phthalocyanines 17 (2013) 1094–1103.
[30] A.H. Corwin, A.B. Chivvis, R.W. Poor, D.G. Whitten, E.W. Baker, J. Am. Chem. Soc. 90 (1968) 6577–6583.
[31] W.S. Caughey, R.M. Deal, C. Weiss, M. Gouterman, J. Mol. Spectrosc. 16 (1965) 451–463.
[32] R.E. Haddad, S. Gazeau, J. Pécaut, J.-C. Marchon, C.J. Medforth, J.A. Shelnutt, J. Am. Chem. Soc. 125 (2003) 1253–1268.
[33] P.G. Plieger, A.K. Burrell, S.B. Hall, D.L. Officer, J. Incl. Phenom. Macrocycl. Chem. 53 (2005) 143–148.
[34] D. Skrzypek, I. Madejska, J. Habdas, Solid State Sci. 9 (2007) 295–302.
[35] M. Aydin, Vib. Spectrosc. 68 (2013) 141–152.
[36] A. Fidalgo-Marijuan, G. Barandika, B. Bazan, M.-K. Urtiaga, M.I. Arriortua, Cryst. Eng. Commun. 15 (2013) 4181–4188.
[37] S.D. Gokakakar, A.V. Salker, J. Thermal Anal. Calorim. 109 (2012) 1487–1492.
[38] S.D. Gokakakar, A.V. Salker, J. Thermal Anal. Calorim. 101 (2010) 809–813.
[39] K.M. Kadish, E. Van Caemelbecke, J. Solid State Electrochem. 7 (2003) 254–258.
[40] J.H. Fuhrhop, D. Mauzerall, J. Am. Chem. Soc. 91 (1969) 4174–4181.
[41] K.M. Kadish, M.M. Morrison, J. Am. Chem. Soc. 98 (1976) 3326–3328.
[42] K.M. Kadish, R.K. Rhodes, Inorg. Chem. 20 (1981) 2961–2966.
[43] K.M. Kadish, E.V. Caemelbecke, Encyclopedia of Electrochemistry, Wiley-VCH Verlag GmbH & Co KGaA, 2007.
[44] K.M. Kadish, K.M. Smith, R. Guilard, The Porphyrin Handbook: Electron Transfer, Academic Press, 2000.
[45] Y. Li, Y. Cao, J. Gao, D. Wang, G. Yu, A.J. Heeger, Synth. Met. 99 (1999) 243–248.